materials

MDPI

Article

Magnetic Behavior in TiS_3 Nanoribbon

Shengqiang Lai [1] and Yongping Du [2,*]

[1] The School of Physics, Nanjing University, Nanjing 210093, China; lai@smail.nju.edu.cn
[2] Department of Applied Physics and Institution of Energy and Microstructure, Nanjing University of Science and Technology, Nanjing 210094, China
* Correspondence: njustdyp@njust.edu.cn

Received: 9 September 2019; Accepted: 22 October 2019; Published: 25 October 2019

Abstract: The electronic structure, magnetic properties and strain response of N-a-TiS_3 nanoribbons are investigated by first-principles calculations. We find that the magnetic ground state is strongly dependent on width of **a**-TiS_3. When N equals an odd number the ground state is a ferromagnetic (FM) metal, meanwhile, when N equals an even number the ground state is an anti-ferromagnetic (AFM) metal. More interestingly, a tensile strain as large as 6% can tune the 9-**a**-TiS_3 nanoribbon from a FM metal to a half metal. A 4% tensile strain also causes a phase transition from AFM to FM ground state for 10-**a**-TiS_3 nanoribbon. Our findings show that N-**a**-TiS_3 is a promising candidate for spintronic and electronic applications.

Keywords: TiS_3; nanoribbon; magnetic property; strain effect

1. Introduction

The properties of materials are essentially associated with dimensionality. Due to low dimensionality, quantum confinement and their promising applications in spintronics, optronics, thermoelectrics [1–4], etc., one-dimensional (1D) nanostructures, such as nanotubes, nanowires, nanobelts, and nanoribbons, have drawn a lot of attention during the past two decades [5–7]. When graphene is cut into 1D graphene nanoribbons, even more fantastic properties are predicted and some have already been verified experimentally [8–11]. Especially, the zigzag graphene nanoribbons (ZGNRs) were predicted to be antiferromagnetic semiconductors [12,13]. More interestingly, many theoretical studies have demonstrated that the half-metallicity in ZGNRs can be realized under external transverse electric fields [14,15], or by selective chemical modifications [16–18]. Many other methods, like doping [17] or defects [19], were applied to tune or control the magnetism in ZGNRs. Moreover, ZGNRs can carry a spin current response to an external electric field, which opens a new path to the application of spintronics [14]. In addition to ZGNRs, magnetism hasalso been predicted in many other nanoribbons, such as CoTe [1], Fe_2GeAl [2], MnSi [3], BN [20], MoS_2 [21], black and blue phosphorus [22,23], andZnO [24].

Very recently, a new two-dimensional (2D) material, namely TiS_3, has been successfully synthesized [25–28]. It is reported that monolayer TiS_3exhibits a direct band gap of 1.1–1.2 eV [29], making the bandgap of TiS_3 comparable to that of silicon (1.1 eV). Also, numerical results show that the bandgap of TiS_3 is quite robust, almost independent of layer thickness, vertical strain and stacking order [30]. Moreover, a recent theoretical study proposed that TiS_3 is expected to have a higher electron mobility of 10,000 $cm^2V^{-1}s^{-1}$ [29]. Such a robust bandgap and ultrahigh electron mobility make TiS_3 a good candidate for nanoelectronics and optoelectronics application. The elastic modulus, carrier mobility and band structure of TiS_3 are strongly anisotropic due to its highly anisotropic crystal. Experimentally, nanoribbons of TiS_3 were successfully prepared [25–28]. Although, there are several studies on nanoribbons of TiS_3 [25–28,31–33], the magnetism of TiS_3 nanoribbon still lacks systematic study.

In this article, using first-principles calculation, we systematically study the magnetic properties of TiS_3 nanoribbon. Our results show that **a**-TiS_3 NR is a spin-polarized metal with local magnetic moments at the edge, while **b**-TiS_3 NR is nonmagnetic semiconductor. More interestingly, the magnetic ground state of N-**a**-TiS_3 NRs (N = 7, 8, 9, 10, 11) are width dependent. When N is odd, the ground state is ferromagnetism (FM), meanwhile the ground state is anti-ferromagnetism (AFM)when N is even. This magnetic behavior is very different from other magnetic nanoribbons, such as zigzag black phosphorene nanoribbons [22] and zigzag graphene nanoribbons [12,13], whose magnetic properties are almost independent on the width of nanoribbon. We also find that compressive strain almost does not change the magnetic and electric properties of **a**-TiS_3 NRs. However, according to our calculations in 9-**a**-TiS_3 NR and 10-**a**-TiS_3, tensile strain can change the magnetic and electric properties dramatically. 9-**a**-TiS_3 NR becomes a half metal under a tensile as large as 6%, and the AFM ground state of 10-**a**-TiS_3 is tuned into a FM ground state at about 4% tensile strain. Our findings show that the a-TiS_3 NRs are promising candidates for spintronics and electronics application.

2. Methods

All the calculations were carried with Vienna ab initio Simulation Package (VASP, version 5.3.2, University of Vienna, Vienna, Austria) [34,35]. The frozen-core projector augmented wave (PAW) method and the generalized gradient approximation (GGA) of Perdew–Burke–Ernzerhof (PBE) [36] were adopted. Cutoff energy was set as 500 eV for plane-wave expansion of the electronic wave function, and appropriate k-point meshes ($9 \times 1 \times 1$) were used for geometric optimization and self-consistent calculation. All structures were relaxed until the force on each atom was less than 0.01 eV/ Å. The energy convergence criteria were set to 1.0×10^{-6} eV. A vacuum spacing of 15 Å was used so that the interaction in the non-periodic directions can be neglected. Since both Ti and S are not heavy elements, spin-orbit coupling (SOC) is expected to be small, thus the spin-orbit interaction is not included in all calculations.

3. Results and Discussion

The unit cell of monolayer TiS_3 is a rectangle. Our optimized lattice constants are a = 5.02 Å, b = 3.40 Å which are in good agreement with previous experimental result (4.96 and 3.40 Å) [37], and theoretical result (5.02 and 3.41 Å) [31]. There are two particular ways to cut monolayer TiS_3 into nanoribbons (cutting along the **a** axis or **b** axis). Then, two types of nanoribbons are indicated as N-**a**-TiS_3 NR and N-**b**-TiS_3 NR, where N indicates the number of Ti atoms in the unit cell of ribbon and **a**-TiS_3 NR and **b**-TiS_3 NR are along the **a** and **b** lattice vectors, respectively. Our calculations show that N-**b**-TiS_3 NRs are semiconductors without any local magnetic moment, which is consistent with previous theoretical results [31]. Thus, in the following discussion we will eliminate the N-**b**-TiS_3 NRs and mainly consider the N-**a**-TiS_3 NRs.

Here, we take N = 7–11 for a-TiS_3 NRs. Figure 1 shows the crystal structure of 10-**a**-TiS_3 NR and 9-**a**-TiS_3 NR. In particular, edge atoms may influence the physical properties. For **a**-TiS_3 NR, the edge atoms are S and Ti with dangling bonds which are local states around Fermi level as shown later. However, there are some differences in crystal structure between 9-**a**-TiS_3 NR and 10-**a**-TiS_3 NR. Dashed lines in Figure 1a,b also indicate the TiS_3 chain in monolayer TiS_3. In 9-**a**-TiS_3 NR, the terminal atoms for every TiS_3 chain are the same, namely both of two edge atoms are Ti or S atoms for the same chain as shown in Figure 1b. However, in 10-**a**-TiS_3 NR, the edge atoms for every TiS_3 chain are different, i.e., one terminal atom is Ti and the other is an S atom shown in Figure 1a. Moreover, for N equal to all other odd numbers (or even numbers) the edge atom arrangement is the same as the N = 9 (or 10). This different edge atom arrangement will cause a different magnetic ground state of two NRs as discussed below.

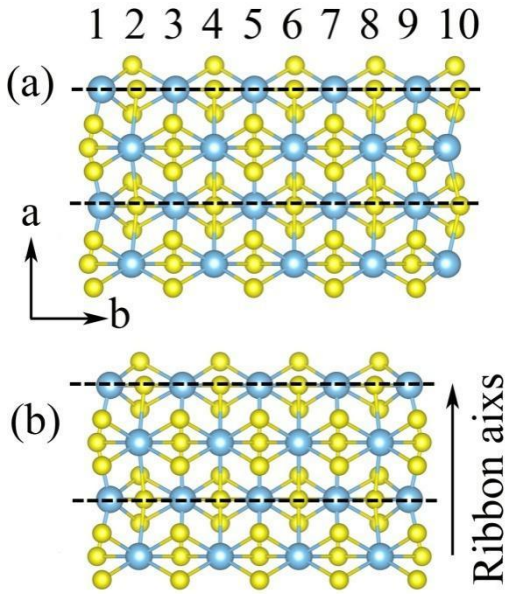

Figure 1. (**a**) The crystal structure of 10-**a**-TiS_3nanoribbon (NR), and; (**b**) the crystal structure of 9-**a**-TiS_3. Two dashed lines indicate the unit cell of nanoribbon along the a lattice vector. The dashed lines indicate the TiS_3 chain in monolayer TiS_3.

Firstly, we calculate the electronic structure of 9-**a**-TiS_3 NR and 10-**a**-TiS_3 NR under GGA approximation without any spin polarization. The electronic structures of two nanoribbons are shown Figure 2. Three bands, denoted by red color, cross the Fermi energy indicating the metallic behavior of **a**-TiS_3 NR (shown in Figure 2a,e). Further analysis shows that these three bands are the edge states. Density of states (DOS), shown in Figure 2, indicate that three bands crossing the Fermi level are mainly contributed by the unbonding p_y and p_z states of edge S atoms and d_{z^2} and $d_{x^2-y^2}$ of edge Ti atoms. A peak of DOS near the Fermi energy, as shown in total DOS, indicates the possibility of spin polarization driven by Stoner instability [38].

To clarify the effect of edge atoms, we plot the charge density isosurfaces of these three bands which cross the Fermi energy and the results are shown in Figure 2i–l. These pictures clearly illustrate the charge density is mainly localized at edge S and Ti atoms which again proves that three bands denoted by red lines are indeed the edge states. As we discussed before, the arrangement of edge atoms is different between 9-**a**-TiS_3 NR and 10-a-TiS_3 NR. Thus, charge distribution is different for these two **a**-TiS_3 NRs. In 9-**a**-TiS_3 NR, the charges are mainly localized at edge S atoms which are in the TiS_3 chain, whose the end atoms are both sulfur atoms, shown in Figure 2i,j. The p orbital shape of charge density on edge S atoms are the hybridization of p_y and p_z unbonding state. However, the contribution of Ti-d state in TiS_3 chain with two end Ti atoms is more complicated. The charge distribution shows that all Ti atoms in this chain have almost equal contributions to the three red bands. This means that the hybridization between Ti atoms is very strong. However, there is a very different charge distribution in 10-**a**-TiS_3 NR. As we discussed previously, the terminals of TiS_3 chain were one S atom and one Ti atom, rather than the two same atoms. Thus, the charge distribution of 10-**a**-TiS_3 NR is very different from that of 9-**a**-TiS_3 NR. In Figure 2k,l, we can see that there are p orbital shapes of charge density around edge S atoms, as in 9-**a**-TiS_3 NR. More interestingly, the charge distribution on Ti atoms in the same chain are not equal at all. The biggest contribution comes from the edge Ti atom, and then the charge density decreases from the edge Ti atom to other side of NR which is different from the situation in 9-**a**-TiS_3 NR. As we discuss later, this difference would cause the different magnetic ground states.

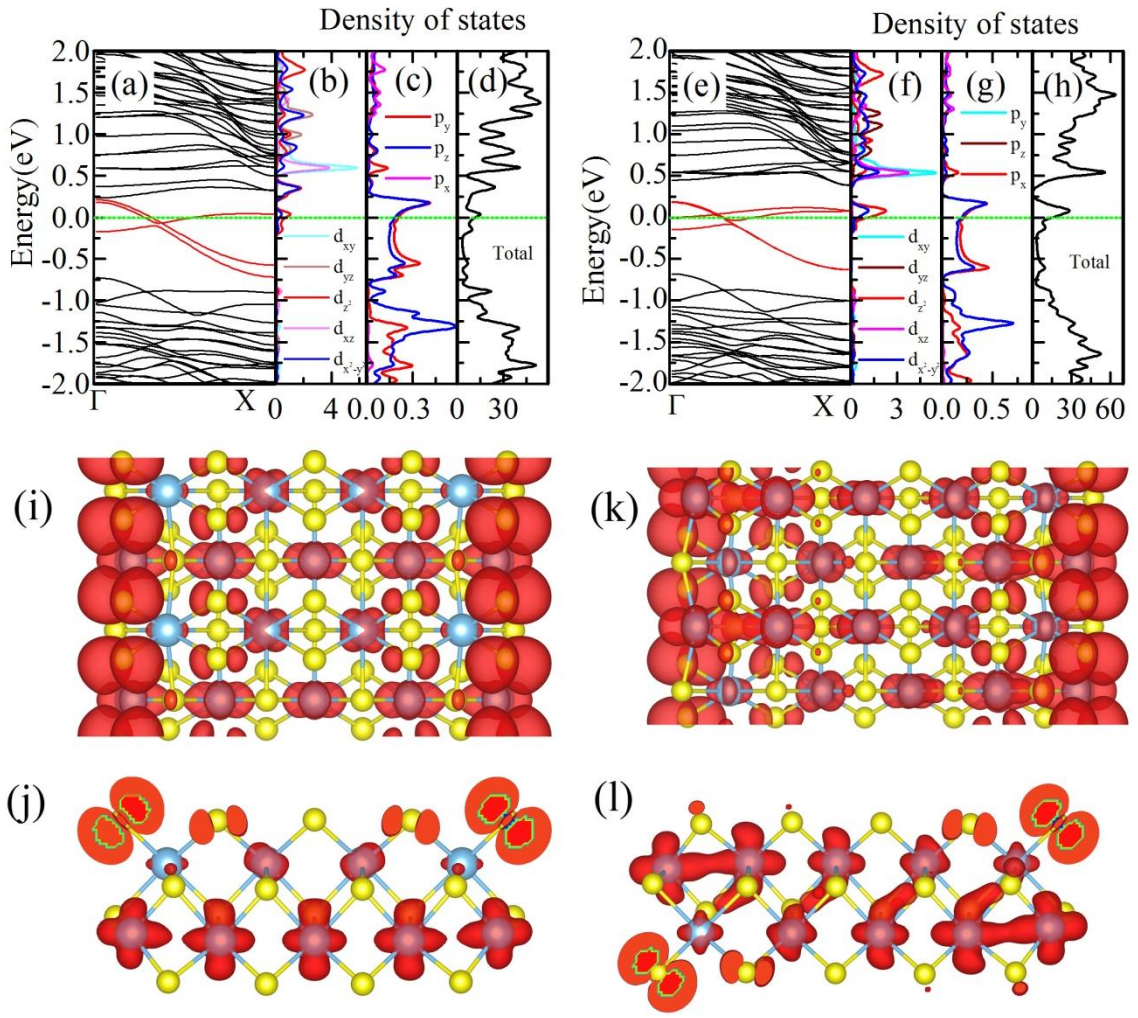

Figure 2. (**a**) and (**e**) are the band structures of 9-**a**-TiS_3 NR and 10-a-TiS_3, respectively, within the GGA calculation. Three bands, which cross the Fermi level and are denoted by red color, are the edge states. (**b**) and (**f**) are the density of states of d-orbital of edge Ti atoms in 9-**a**-TiS_3 NR and 10-a-TiS_3 NR respectively. (**c**) and (**g**) are the density of states of p-states of edge S atoms in 9-**a**-TiS_3 and 10-**a**-TiS_3 NRs; (**d**) and (**h**) are the total density of states of 9-**a**-TiS_3 and 10-**a**-TiS_3 NRs respectively. (**i**) and (**j**) are the charge density of three red bands of 9-**a**-TiS_3 NR. (**k**) and (**l**) are the charge density of three red bands of 10-**a**-TiS_3 NR. (**i**) and (**k**) are the top view while (**j**) and (**l**) are the side view along the period direction.

The previous theoretical study has proposed that the **a**-TiS_3 NRs have local magnetic moment [31]. But detailed studies of magnetic properties are still lacking. Thus, we perform the spin-polarized calculation to find the magnetic properties of N-**a**-TiS_3 NRs.

To explore the magnetic ground state of N-**a**-TiS_3 NRs, we set two magnetic configurations, one is a FM arrangement with all magnetic moments in the same direction and the other is an AFM configuration with the magnetic moments of the two edges anti-parallel. From the results of the total energy calculation, we can easily find that the ground state of N-**a**-TiS_3 NRs are not all FM which is different from the previous theoretical results [31]. The magnetic ground state varies as the width changes. Figure 3a shows that the energy difference between the magnetic state and nonmagnetic state, one can easily see that when N is odd, the ground state is FM, meanwhile N is even, the ground state is AFM. This width-dependent magnetic ground state is different from other 2D material NRs like black phosphorus [23].

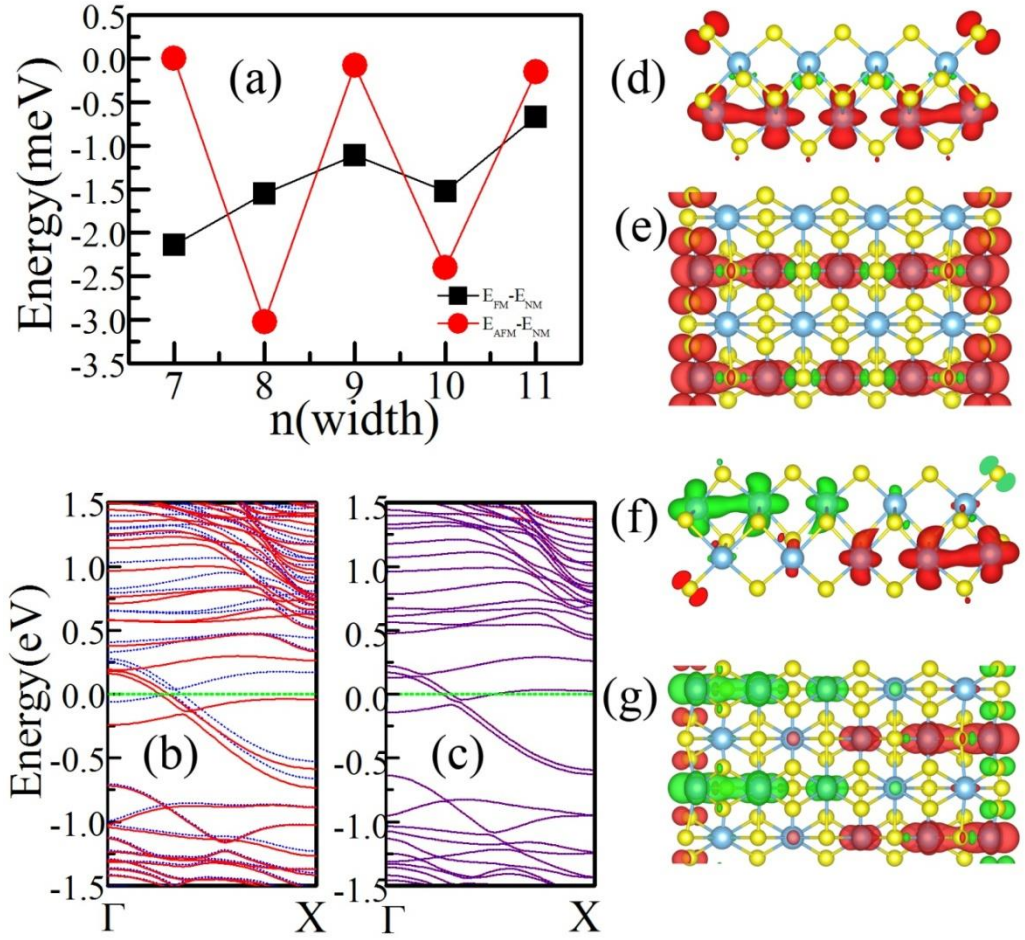

Figure 3. (**a**) The energy of magnetic ground state changes as the width of **a**-TiS_3 NR. (**b**) The spin-polarized band structure of the FM ground state of 9-**a**-TiS_3 NR, red lines (blue dashed lines) indicate spin up (down) component. (**c**) The spin-polarized band structure of AFM ground state of 10-**a**-TiS_3, red lines (blue dashed lines) denote spin up (down) component. (**d**) and (**e**) are spin density of FM state of 9-**a**-TiS_3 NR, (**d**) is the side view from the period direction of **a**-TiS_3 NR and (**e**) is the top view. (**f**) and (**g**) are the spin density of the AFM state of 10-**a**-TiS_3 NR, (**f**) is side view from the period direction of 10-**a**-TiS_3 NR and (**g**) is the top view.

Our calculations also reveal that all N-**a**-TiS_3 NRs have metallic behavior with bands crossing the Fermi level. The electronic band dispersion of ground magnetic states of 9-**a**-TiS_3 NR and 10-**a**-TiS_3NR are shown in Figure 3b,c, respectively. For FM ground state of 9-**a**-TiS_3, there is a spin split near the Fermi level. The total magnetic moment of the unit cell is 0.86 μB which is consistent with the previous calculation [31]. Due to the AFM ground state, two spin components of 10-**a**-TiS_3 are exactly overlapped indicating a perfect AFM state. We also checked the effect of SOC, and we found that the SOC does not change the magnetic ground states of N-a-TiS3 NRs, due to the small SOC effect in light elements.

To get further insight into the spin polarization in **a**-TiS_3 NRs, we also calculated the spin density, which is the difference between spin-up and spin-down channels, and show them in Figure 3d–g. Figure 3d,e are the spin density of FM 9-**a**-TiS_3 NR. The magnetic moment is mainly located on edge S and edge Ti atoms; in addition, the magnetic moment is still located in Ti atoms in the TiS_3 chain whose terminal atoms are Ti atom. The magnetic moment decreases from 0.144 μB (edge Ti atom) to 0.131 μB (center Ti atom). The distribution of magnetic moment also indicates the strong hybridization between Ti atoms. Figure 3f,g are the spin density of 10-**a**-TiS_3 NR in AFM ground state. The magnetic moment

is mainly located at edge S atoms and Ti atoms. Due to the strong hybridization between Ti atoms in the same TiS_3 chain, magnetic moments turn to zero gradually from the terminal Ti to center one.

As is well known, the edge states usually are sensitive to strain, doping, and the external field. Here we focused on the effect of strain on the edge states. A uniaxial strain varying from −6% to 6% was applied to investigate the magnetic and electronic properties. The energy differences between FM and nonmagnetic/AFM states of 9-a-TiS_3 NR (10-a-TiS_3 NR) are shown in Figure 4a. We found that for both 9 and 10-a-TiS_3 NR, the compressive strains have a small effect on the magnetic ground state. Although the FM ground state is not changed by tensile strain, the electronic structure had a dramatic change. We calculated the band structure of 9-a-TiS_3 NR under the various strains, and found that when a tensile strain as large as 6%, FM 9-a-TiS_3 NR become a half metal. The band structure of 9-a-TiS_3 NR under 6% tensile strain is plotted in Figure 4b with the red lines denoting the spin up component and blue dashed lines denoting the spin down component. We can clearly see that the spin-up component opens an indirect band gap about 0.2 eV while three spin-down bands cross Fermi energy indicating metal property. The energy difference between AFM and FM show that there is an AFM-FM phase transition of 10-a-TiS_3 NR under a 4% tensile strain. We also plotted the band structure of 10-a-TiS_3 NR under the 6% tensile strain, a large spin-split around Fermi energy shows the FM property.

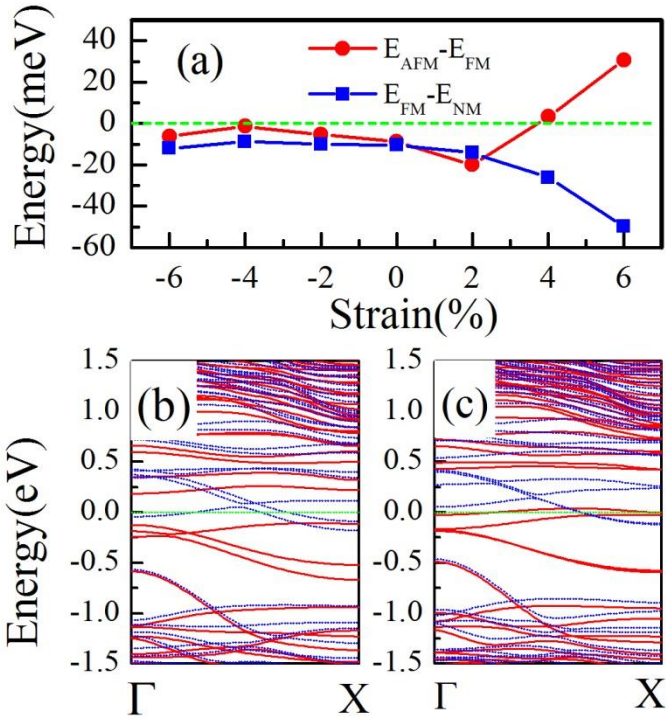

Figure 4. (**a**) Energy difference between nonmagnetic (E_{NM})/anti-ferromagnetic (E_{AFM}) and ferromagnetic (E_{FM}) as a function of strain. (**b**) The spin-polarized band structure of 9-**a**-TiS_3 NR under 6% tensile strain. (**c**) The spin-polarized band structure of 10-**a**-TiS_3 NR under 6% tensile strain.

4. Conclusions

In summary, we investigated the electronic and magnetic properties of TiS_3 NRs and strain effect by first-principles calculations. Our results reveal that b-TiS_3 NRs are non-magnetic semiconductors consistent with previous results. However, the magnetic ground states of N-a-TiS_3 NRs are strongly dependent on the width of NRs. When N is an (even) odd number, N-a-TiS_3 NRs are (anti-)ferromagnetic metals. The strain effect is also investigated. The compressive strain has little effect on the electronic and magnetic properties of 9(10)-a-TiS_3 NRs. On the contrary, a 6% tensile strain will tune 9-a-TiS_3

NR from a FM metal into a half metal while a 4% tensile strain cause a AFM-FM phase transition of 10-a-TiS_3 NR. Our findings make the N-a-TiS_3 NRs promising spintronic devices.

Author Contributions: S.L. performed the calculations; Y.D. interpreted the numerical results and wrote the paper.

Funding: The authors gratefully acknowledge support from the Jiangsu Province Science Foundation for Youth (Grant No. BK20170821) and National Science Foundation of China for Youth (Grant No. 11804160).

Conflicts of Interest: The authors declare no conflicts of interest.

References

1. Dahal, B.R.; Dulal, R.P.; Pegg, I.L.; Philip, J. Electrical transport and magnetic properties of cobalt telluride nanostructures. *J. Vac. Sci. Technol. B* **2016**, *34*, 051801. [CrossRef]
2. Dulal, R.P.; Dahal, B.R.; Forbes, A.; Bhattarai, N.; Pegg, I.L.; Philip, J. Ferromagnetism in Fe_2XrAl nanowires. *J. Vac. Sci. Technol. B* **2018**, *36*, 022902. [CrossRef]
3. Liang, D.; DeGrave, J.P.; Stolt, M.J.; Tokura, Y.; Jin, S. Current-driven dynamics of skyrmions stabilized in MnSi nanowires revealed by topological Hall effect. *Nat. Commun.* **2015**, *6*, 8217. [CrossRef] [PubMed]
4. Stano, M.; Fruchart, O. Magnetic Nanowires and Nanotubes. *Handb. Magn. Mater.* **2018**, *27*, 155–267.
5. Novoselov, K.S.; Geim, A.K.; Morozov, S.V.; Jiang, D.; Zhang, Y.; Dubonos, S.V.; Grigorieva, I.V.; Firsov, A.A. Electric Field Effect in Atomically Thin Carbon Films. *Science* **2004**, *306*, 666. [CrossRef]
6. Zhang, Y.; Tan, Y.; Stormer, H.; Kim, P. Experimental observation of the quantum Hall effect and Berry's phase in graphene. *Nature* **2005**, *438*, 201. [CrossRef]
7. Xia, Y.; Yang, P.; Sun, Y.; Wu, Y.; Mayers, B.; Gates, B.; Yin, Y.; Kim, F.; Yan, H. Mediated Synthesis of Fe_2O_3 Nanorods. *Adv. Mater.* **2003**, *15*, 353. [CrossRef]
8. Barone, V.; Hod, O.; Scuseria, G.E. Electronic Structure and Stability of Semiconducting Graphene Nanoribbons. *Nano Lett.* **2006**, *6*, 2748–2754. [CrossRef]
9. Son, Y.-W.; Cohen, M.L.; Louie, S.G. Energy gaps in graphene nanoribbons. *Phys. Rev. Lett.* **2006**, *97*, 216803. [CrossRef]
10. Han, M.Y.; Özyilmaz, B.; Zhang, Y.; Kim, P. Energy Band-Gap Engineering of Graphene Nanoribbons. *Phys. Rev. Lett.* **2007**, *98*, 206805. [CrossRef]
11. Li, X.L.; Wang, X.R.; Zhang, L.; Lee, S.W.; Dai, H.J. Chemically derived, ultrasmooth graphene nanoribbon semiconductors. *Science* **2008**, *319*, 1229–1232. [CrossRef] [PubMed]
12. Fujita, M.; Wakabayashi, K.; Nakada, K.; Kusakabe, K.J. Physical Peculiar localized state at zigzag graphite edge. *Soc. Jpn.* **1996**, *65*, 1920–1923. [CrossRef]
13. Nakada, K.; Fujita, M.; Dresselhaus, G.; Dresselhaus, M.S. Edge state in graphene ribbons: Nanometer size effect and edge shape dependence. *Phys. Rev. B* **1996**, *54*, 17954–17961. [CrossRef] [PubMed]
14. Son, Y.-W.; Cohen, M.L.; Louie, S.G. Half-metallic graphene nanoribbons. *Nature* **2006**, *444*, 347–349. [CrossRef] [PubMed]
15. Hod, O.; Barone, V.; Peralta, J.E.; Scuseria, G.E. Enhanced half-metallicity in edge-oxidized zigzag graphene nanoribbons. *Nano Lett.* **2007**, *7*, 2295–2299. [CrossRef]
16. Kan, E.J.; Li, Z.Y.; Yang, J.L.; Hou, J.G. Half-metallicity in edge-modified zigzag graphene nanoribbons. *J. Am. Chem. Soc.* **2008**, *130*, 4224–4225. [CrossRef] [PubMed]
17. Li, Y.F.; Zhou, Z.; Shen, P.W.; Chen, Z.F. Spin Gapless Semiconductor−Metal−Half-Metal Properties in Nitrogen-Doped Zigzag Graphene Nanoribbons. *ACS Nano* **2009**, *3*, 1952–1958. [CrossRef]
18. Dutta, S.; Pati, S.K. Half-metallicity in undoped and boron doped graphene nanoribbons in the presence of semilocal exchange-correlation interactions. *J. Phys. Chem. B* **2008**, *112*, 1333–1335. [CrossRef]
19. Lin, X.; Ni, J. Half-metallicity in graphene nanoribbons with topological line defects. *Phys. Rev. B* **2011**, *84*, 075461. [CrossRef]
20. Barone, V.; Peralta, J.E. Magnetic boron nitride nanoribbons with tunable electronic properties. *Nano Lett.* **2008**, *8*, 2210–2214. [CrossRef]
21. Li, Y.F.; Zhou, Z.; Zhang, S.B.; Chen, Z.F. MoS_2 Nanoribbons: High Stability and Unusual Electronic and Magnetic Properties. *J. Am. Chem. Soc.* **2008**, *130*, 16739. [CrossRef] [PubMed]
22. Hu, T.; Hong, J. Electronic structure and magnetic properties of zigzag blue phosphorene nanoribbons. *J. Appl. Phys.* **2005**, *118*, 054301. [CrossRef]

23. Du, Y.P.; Liu, H.M.; Xu, B.; Sheng, L.; Yin, J.; Duan, C.G.; Wan, X.G. Unexpected Magnetic Semiconductor Behavior in Zigzag Phosphorene Nanoribbons Driven by Half-Filled One Dimensional Band. *Sci. Rep.* **2015**, *5*, 8921. [CrossRef] [PubMed]
24. Botello-Méndez, A.R.; Loópez-Uriías, F.; Terrones, M.; Terrones, H. Magnetic Behavior in Zinc Oxide Zigzag Nanoribbons. *Nano Lett.* **2008**, *8*, 1562.
25. Island, J.O.; Buscema, M.; Barawi, M.; Clamagirand, J.M.; Ares, J.R.; Sanchez, C.; Ferrer, I.J.; Steele, G.A.; van der Zant, H.S.J.; Castellanos-Gomez, A. Ultrahigh Photoresponse of Few-Layer TiS_3 Nanoribbon Transistors. *Adv. Opt. Mater.* **2014**, *2*, 641–645. [CrossRef]
26. Island, J.O.; Buscema, M.; Biele, R.; Almazan, A.; Clamagirand, J.M.; Ares, J.R.; Sanchez, C.; van der Zant, H.S.; Álvarez, J.V.; D'Agosta, R.; et al. TiS_3 Transistors with Tailored Morphology and Electrical Properties. *Adv. Mater.* **2015**, *27*, 2595–2601. [CrossRef]
27. Pawbake, A.S.; Island, J.O.; Flores, E.; Ares, J.R.; Sanchez, C.; Ferrer, I.J.; Jadkar, S.R.; van der Zant, H.S.; Castellanos-Gomez, A.; Late, D.J. Temperature-Dependent Raman Spectroscopy of Titanium Trisulfide (TiS_3) Nanoribbons and Nanosheets. *ACS Appl. Mater. Interfaces* **2015**, *7*, 24185–24190. [CrossRef]
28. Molina-Mendoza, A.J.; Barawi, M.; Biele, R.; Flores, E.; Ares, J.R.; Sanchez, C.; Rubio-Bollinger, G.; Agrat, N.; D'Agosta, R.; Ferrer, I.J.; et al. Electronic Bandgap and Exciton Binding Energy of Layered Semiconductor TiS_3. *Adv. Electron. Mater.* **2015**, *1*, 1500126. [CrossRef]
29. Dai, J.; Zeng, X.C. Titanium trisulfide monolayer: Theoretical prediction of a new direct-gap semiconductor with high and anisotropic carrier mobility. *Angew. Chem.-Int. Ed.* **2015**, *54*, 7572. [CrossRef]
30. Kang, J.; Wang, L.W. Robust band gap of TiS_3 nanofilms. *Phys. Chem. Chem. Phys.* **2016**, *18*, 14805. [CrossRef]
31. Kang, J.; Sahin, H.; Ozaydin, D.; Senger, R.T.; Peeters, F.M. TiS_3 nanoribbons: Width-independent band gap and strain-tunable electronic properties. *Phys. Rev. B* **2015**, *92*, 075413. [CrossRef]
32. Ce, H.; Zhang, E.Z.; Yuan, X.; Wang, W.Y.; Liu, Y.W.; Zhang, C.; Ling, J.W.; Liu, S.S.; Xiu, F.X. Tunable charge density wave in TiS_3 nanoribbons. *Chin. Phys. B* **2017**, *26*, 067302. [CrossRef]
33. Lipatov, A.; Loes, M.J.; Lu, H.D.; Dai, J.; Patoka, P.; Vorobeva, N.S.; Muratov, D.S.; Ulrich, G.; Kästner, B.; Hoehl, A.; et al. Quasi-1D TiS_3 Nanoribbons: Mechanical Exfoliation and Thickness-Dependent Raman Spectroscopy. *ACS Nano* **2018**, *12*, 12713–12720. [CrossRef] [PubMed]
34. Kresse, G.; Hafner, J. Ab initio molecular dynamics for liquid metals. *Phys. Rev. B* **1993**, *47*, 558(R). [CrossRef] [PubMed]
35. Kresse, G.; Furthmuller, J. Efficient iterative schemes for ab initio total-energy calculations using a plane-wave basis set. *Phys. Rev. B* **1996**, *54*, 11169. [CrossRef]
36. Perdew, J.P.; Burke, K.; Ernerhof, M. Generalized Gradient Approximation Made Simple. *Phys. Rev. Lett.* **1997**, *77*, 3865. [CrossRef]
37. Furuseth, S.; Brattas, L.; Kjekshus, A. Crystal Structures of TiS_3, ZrS_3, $ZrSe_3$, $ZrTe_3$, HfS_3 and $HfSe_3$. *Acta Chem. Scand.* **1975**, *29*, 623.
38. Stoner, E.C. Collective electron specific heat and spin paramgnetism in metals. *Proc. R. Soc. A* **1936**, *154*, 656.